UNIVERSITYOF BIRMINGHAM
University of Birmingham Research at Birmingham

Influence of the kissing bond on the mechanical properties and fracture behaviour of AA5083-H112 friction stir welds

Zhou, Nan; Song, Dongfu; Qi, Wenjun; Li, Xiaohui; Zou, Ji; Attallah, Moataz M.

Link to publication on Research at Birmingham portal

Influence of the Kissing Bond on the Mechanical Properties and Fracture Behaviour of AA5083-H112 Friction Stir Welds

Nan Zhou[1,2,3], Dongfu Song[1,3], Wenjun Qi[1], Xiaohui Li[1,3], Ji Zou[2], Moataz M. Attallah[2],

1, Guangdong Institute of Materials and Processing, Guangzhou 510650, China

2, School of Metallurgy and Materials, University of Birmingham, Edgbaston, Birmingham B15 2TT, UK

3: Guangdong Provincial Key Laboratory for Technology and Application of Metal Toughening, Guangzhou 510650, China

ABSTRACT

The kissing bond phenomenon in AA5083-H112 friction stir butt welds was investigated in joints welded using a matrix of welding parameters, with tool rotation speeds of 800, 1000, and 1200 rpm and feed speeds 100, 200, and 300 mm/min. The length of the kissing bond along the cross-section normal to the welding direction was measured to quantify its influence on the mechanical properties. A combination of optical microscopy, scanning electron microscopy, transmission electron microscopy, tensile and fatigue testing were used to elucidate the impact of the kissing bond on the microstructural and mechanical properties development. The fracture type, location, and morphology were studied for the various conditions. The results showed that the welding parameters had a substantial effect on the length of the kissing bond, which was found to decrease with the increase in the welding heat input, as estimated based on the rotation and feed speeds. Moreover, the length and morphology of the kissing bond had a significant influence on the tensile and fatigue fracture type. A shear fracture type was characteristic for welds showing high tensile properties and long fatigue life, whereas fracture along the kissing bond was characteristic for poor tensile properties and short fatigue life.

KEYWORDS:

Friction stir welding; Kissing bond; Fatigue; Tensile properties; Fracture

1. Introduction

AA5083 is a 5xxx-series work-hardenable alloy that is frequently used in structural

automotive components (body-in-white) due to its high strength-to-weight ratio, good corrosion resistance, and reasonable formability among the commercial Al-alloys [1, 2]. Nonetheless, it is rather difficult to obtain mechanically and metallurgically sound welds using fusion welding technology for this alloy, which limits its application in large scale fabricated vehicle structures [3]. This concern has been overcome using friction stir welding (FSW) technology, which has been successfully applied for 5xxx-series alloys. As a solid state joining technology, FSW would normally result in temperatures lower than the incipient melting temperature ($\sim 600\,°C$ in 5xxx-series alloys) [4].

The effect of FSW process parameters on the mechanical properties and the microstructure of AA5083 FSW joints has been widely investigated [5-12]. Peel *et al.* [10] studied the microstructural, mechanical properties, and residual stress development in AA5083 welds produced using different welding parameters, concluding that the weld properties were dominated by the heat input during FSW. Similar conclusions were drawn by Lombard *et al.* [13], who investigated the influence of FSW tool rotation speed and feed speed on the mechanical properties and fatigue life of AA5xxx. Generally, FSW joints are superior to fusion welds, as suggested by Zhou *et al.* [12], who found that the fatigue life of AA 5083 FSW joints was much longer than the pulsed-MIG welds. Other studies developed numerical simulations for FSW of AA5083 in order to predict the microstructural evolution, with an aim to optimise the welding parameters [14].

One of the major concerns associated with FSW of aluminium alloys is the oxide layer (termed the "kissing bond") that is occasionally observed in FSW butt joints [15]. The kissing bond is believed to be deleterious to the mechanical properties of the welds [16-20]. Sato *et al.* [21] investigated the kissing bond in AA1050 FSW joint using transmission electron microscopy (TEM), identifying it to be made out of Al_2O_3 clusters. It was also found in this research that with the increase of FSW heat-input, the oxide clusters would change from a continuous film into discrete particles. Staniek *et al.* [22] also verified the observation of the oxide clusters by SEM and TEM in FSW AA2024-T3 and AlMg2 dissimilar welds. It was suggested that the formation mechanism of the kissing bond was related to the insufficient

break-up of the oxide layer due to the insufficient stretch of the contacting surfaces around the welding pin [17]. As a result, the kissing bond was found to severely affect the fracture behaviour of the FSW joints [23-26]. Staniek *et al.* [22] found that the fracture path occurs exactly along the kissing bond in specific welding conditions. Tao *et al.* [25] found that the fracture path tended to be at the kissing bond at lower tool rotation speeds. Besides, the kissing bond was found to have a profound effect on the fatigue life. Zhou *et al.* [27] compared the fatigue behaviour of AA5083 FS welds at various weld conditions with and without the kissing bond. According to the results, the fatigue life of welds with a kissing bond were 21-43 times shorter than that of the welds that did not display a kissing bond. Le Jolu *et al.* [28] found JLR (Joint Line Remnant), kissing bond and gap-induced defects in FSW joints of an Al–Cu–Li alloy, which had an increasing effect on the fatigue strength of the welds compared to the sound welds. Kadlec *et al.* [18] studied the influence of the size of the kissing bond in FSW AA7475, while, it was found that a large kissing bond did not have a significant effect on the mechanical properties compared to flawless FSW joints. Besides, The kissing bond did not affect the fracture behaviour also in AA2024-T351 FSW weld studied by Zhang *et al.* [29].

Therefore, it appears that the effects of the kissing bond on the mechanical properties and fracture behaviour have still been uncertain, especially in the absence of a reliable method to detect it. Besides, studies on the change in the shape and structure of the kissing bond due to different FSW parameters are limited in the literature. Hence, this study focuses on the influence of the process parameters on kissing bond formation in AA5083 FSW butt joints that were obtained using different tool rotation speeds and tool feed rates. The study also assesses the influence of the kissing bond on the fracture behaviour using tensile and fatigue testing.

2. Experimental

The base material used for FSW in this study was 6 mm thick AA5083-H112 alloy, the chemical composition of which is shown in Table 1. The tensile strength, yield strength, and elongation of the base metal were 335 MPa, 163 MPa, and 20%, respectively.

Table 1 Chemical composition of aluminium alloy for friction stir welding (wt%).

Material	Si	Fe	Cu	Mn	Mg	Zn	Cr	Ti	Others	Al
AA5083	0.4	0.1	0.1	0.6	4.0	0.2	0.15	0.1	≤0.15	Bal.

For welding, the sheets were cut to dimensions of 100 mm (transverse direction) × 200 mm along the welding direction (WD). The welds were produced using an FSW-3LM-4012 FSW machine. Before welding, the surfaces of the sheets were ground and wiped using acetone to get rid of any surface oxide and oil contamination, respectively. The welds were performed using a tool with a 20 mm diameter shoulder and 6 mm pin length; both were made of H13 tool steel. The tool had a triangular conical right-hand thread, with a 2.5° tilt and an anticlockwise rotation. The welds were carried out in three levels of tool rotation speed (800, 1000, 1200 rpm) and three feed speeds (100, 200, and 300 mm/min). The parameters were identified following various trials to establish a process window that achieves sound welds. All the welded sheets were naturally cooled after welding, prior to unclamping them from the machine.

Metallographic specimens were extracted normal to the WD, ground, and polished to 0.05 μm oxide finish. Keller's reagent (3 ml HNO_3, 6 ml HCl, 6 ml HF, and 150 ml distilled H_2O) was used to etch the samples to reveal the kissing bond and surrounding microstructure. For displaying the grain structure, electrolytic-etching was carried out using 10% $HClO_4$ in ethanol for imaging using electron backscattered diffraction (EBSD). The microstructures were examined using a ZEISS Axioskop 2 MAT mot optical microscope (OM). Etched specimens were examined under a JEOL 6060 scanning electron microscope (SEM) and a JEOL 7000 FEG SEM, both operated at 20 kV. A Nova nano FEG SEM equipped with an Oxford INCA crystal EBSD system was used for EBSD image acquisition. The operating parameters of the EBSD were: a 70° tilt angle, a high voltage of 30 kV, a square grid of with a step size of 0.5 μm. The data were analysed using HKL Channel 5 EBSD software. In order to get rid of the noise points, EBSD maps were processed with applying the data cleaning procedure. A JEOL 2100 Transmission electron microscope (TEM) was used to investigate the kissing bond structure. A kissing bond region was extracted and thinned using a FEI Quanta 3D focused ion beam (FIB) system to study its microstructure.

Room temperature tensile test samples were tested in accordance with BS EN 10002-1: 2001 for FSW joints (loaded normal to the WD across the weld nugget) [30]. The tests were carried out on the DNS200 universal tensile machine, with a crosshead speed of 2 mm/min, with 3 replicates. An Instron-8801 fatigue tester was used for testing the fatigue properties of the welds according to ASTM E466-07 [31]. The parameter of the fatigue test was kept constant for all the conditions (sinusoidal wave with the stress ratio R=0.1, the maximum stress 130 MPa, and oscillation frequency 30 Hz). Prior to testing, the surface and edge of the specimens were ground flat to avoid any surface stress concentration.

3. Results

3.1 The kissing bond in the welds

Fig. 1 shows the typical macrostructure of the AA5083 FSW weld, with the stir zone (SZ), thermo-mechanically affected zone (TMAZ), and heat-affected zone (HAZ). The TMAZ/SZ boundary was characterised by a sharp transition typically towards the advancing side (AS), whereas the transition towards the retreating side (RS) was not as clear as in the AS; a typical feature in FSW joints [15]. It was noticed that in the SZ towards the RS, the kissing bond appears as a dark curved line that extends from the centre of the SZ towards the bottom tip of the weld. Several reports in the literature suggest that kissing bond originates from the oxide layer on the initial butt surface, which is broken up during FSW procedure [17]. The morphology of the kissing bond sometimes appear as a zigzag line [32], lazy S [33], or a wavy pattern [17]. Tao *et al.* [25] classified the kissing bond morphology into a "lazy S" and "kissing bond", with the "lazy S" consisting of fine oxide particles, whereas the "kissing bond" contained huge amounts of micro-voids. In this study, the "lazy S" appeared in the middle and upper parts of the SZ shown as A in Fig. 1, whereas the "kissing bond" was located at the root tip of the SZ shown as B in Fig. 1. Fig. 2 (a) and (b) show SEM micrographs of regions A and B in Fig. 1, respectively. In Fig. 2 (a), oxide particles were observed, as well as some particle exfoliation (an etching artefact), while in Fig. 2 (b), a continuous cluster of fine oxide particles were detected. Hence, although the morphologies of the "lazy S" and "kissing bond" are different because of the different stirring (plastic straining) degrees [15], the intrinsic features within them are the same. As such, the term "kissing bond" will be used below to describe both the "lazy S" and "kissing bond" in this
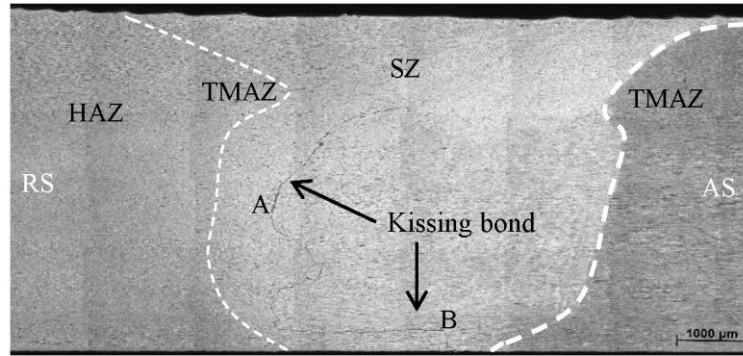
study.

Fig. 1 The weld zones macrostructure of the AA5083 FSW weld.
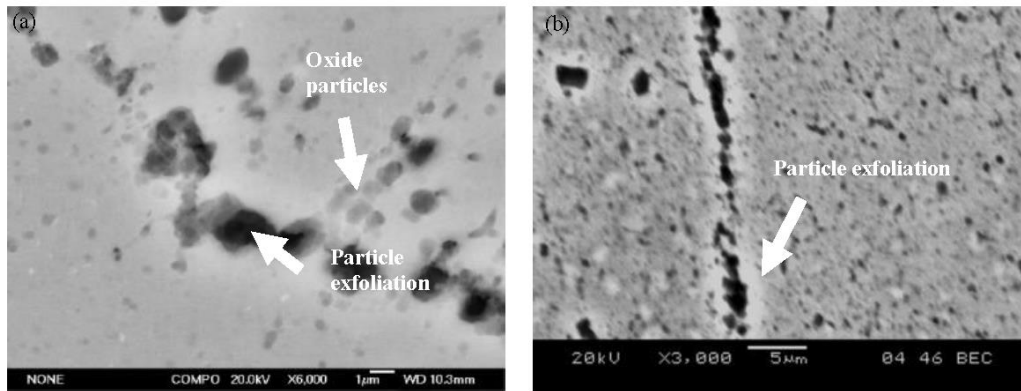(ω=1000rpm, v=300mm/min).

Fig. 2 Backscattered SEM micrographs of (a) zone A and (b) zone B in Fig. 1.

To further clarify the structure of the particles that compose the kissing bond in the SZ of FSW joints, TEM images were taken for the samples that were extracted from the vicinity of kissing bond using FIB. TEM images of the kissing bond of the weld produced at a rotation speed of 1200 rpm and feed speed of 300 mm/min is shown in Fig. 3 (a). The present study observed the local distribution of the bright particles. Many bright particles were locally distributed within the SZ region with an average size ~ 100 nm. It was found that most of the particles were within the grain, while a few of them were on located along the grain boundaries. Energy dispersive X-ray (EDX) spectra obtained from the matrix and the particle are shown in Fig. 3 (b) and (c), respectively. The matrix composition shows ~90 at% Al and 5 at% Mg, with some other elements at less than 5 at%, which are likely due to the FIB process. On the other hand, the particles were found to consist of ~38 at% Al, 12 at% Mg, 48 at% O, and other elements at less than 2 at%. The particles were found to have an extremely higher O content as well as Mg. This result confirmed that the bright particles locally distributed

6

around the kissing bond in AA5xxx-series FSW joints were a mixture of Al_2O_3 and MgO oxides. EBSD mapping shows that the clusters of oxides appear to pin the ground boundaries, creating near-linear boundaries, Fig. 3 (d). The oxide clusters act as a barrier for recrystallisation to progress across the two sides of the kissing bond, which is likely to have an impact on the mechanical performance. This also confirms the view that the kissing bond does not occur in-situ, but is actually due to the residual oxides on the joint interface prior to FSW.
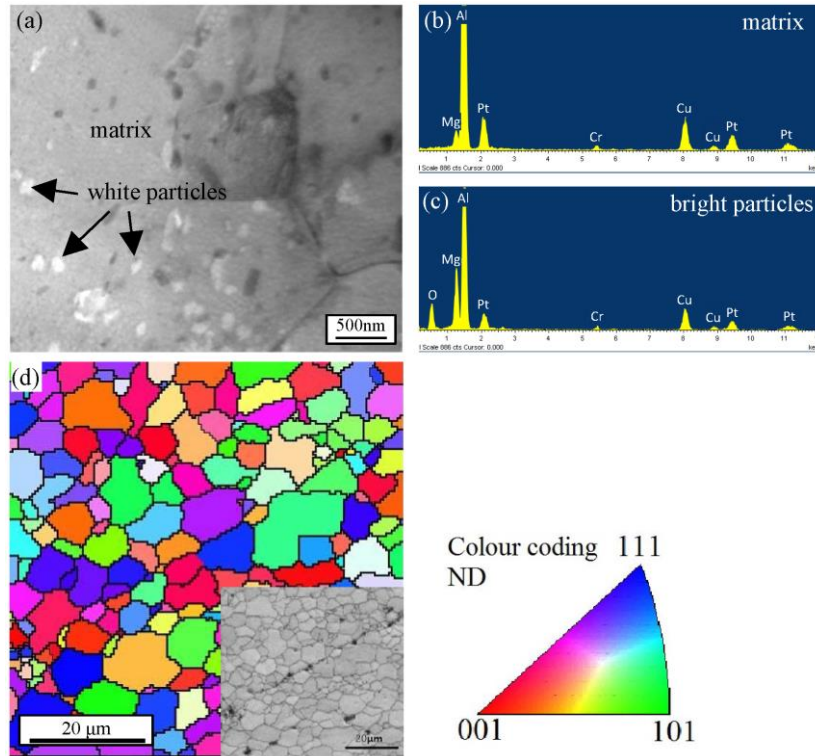

Fig. 3 TEM and EBSD images of the kissing bond.
(a)-TEM image, (b)-EDX spectra of the matrix, (c)- EDX spectra of the particles, (d) EBSD map from the vicinity of the kissing bond.

3.2 Effect of welding parameters on kissing bond

The kissing bond structures formed under different welding parameters investigated in this study are shown in Fig. 4. Fig. 4 (a), (b) and (c) are the welds obtained using different feed rates and the same rotation speed. Fig. 4 (c), (d) and (e) show the welds performed under different tool rotation speeds and the same feed rate. It was found that with the increase in the feed rate, the shape of kissing bond curve changed from a smooth curve pattern to a more complicated zigzag pattern, while with the increase of tool rotation speed, the kissing bond

curve became less pronounced, occupying a narrower region in the lower part of the weld. When the tool rotation speed was 800 rpm, shown in Fig. 4 (c), the kissing bond curve could be observed from the top to the bottom throughout the welds. At 1000 rpm, shown in Fig. 4 (d), the kissing bond curved structure at the top of the welds disappeared, whereas at 1200 rpm, shown in Fig. 4 (e), the bottom part of the kissing bond structure also disappeared. In a word, the welding speed could affect the waviness of the kissing bond, while the tool rotation speed could affect the extent across the weld thickness.
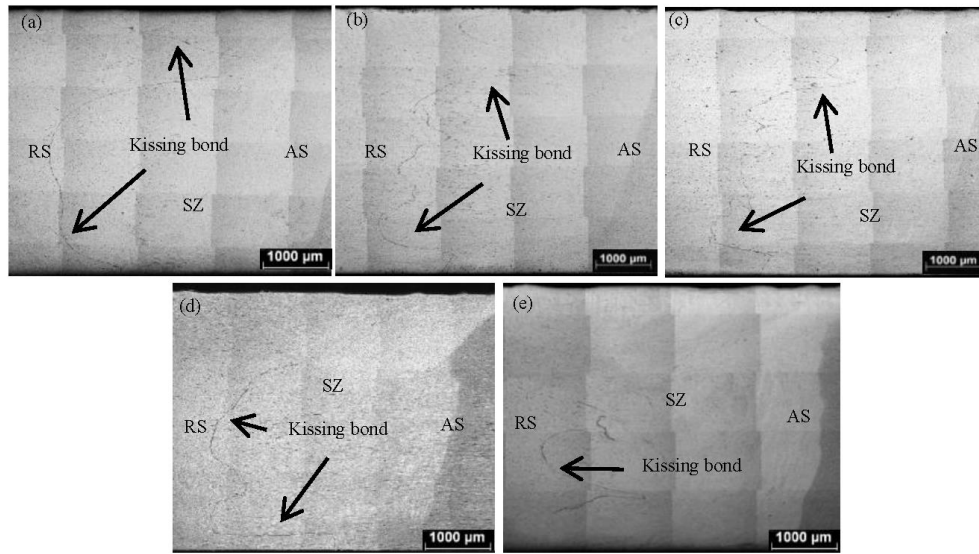

Fig. 4 Macrostructure profiles of the AA5083 FSW welds at different welding parameters.
(a)- ω=800rpm, v=100mm/min, (b)- ω=800rpm, v=200mm/min, (c)- ω=800rpm, v=300mm/min, (d)- ω=1000rpm, v=300mm/min, (e)- ω=1200rpm, v=300mm/min.

In order to further clarify the relation between welding parameters and the kissing bond, the total length of the kissing bond structure (L) was measured using an image analysis software (ImageJ). The relationship between the welding parameters and the length of kissing bond is shown in Fig. 5 (a). When the rotation speed increased, the length of kissing bond was found to decrease, whereas when the feed rate increased, the length was found to increase. During FSW, the oxide film is fragmented by the shear stress produced by the tool rotation speed ω and welding speed v. Thus, the kissing bond is strongly affected by the degree of stirring which is represented by the heat input in the welding procedure.

As FSW is achieved through the combined effect of the tool feed rate and rotation speed, it is essential to consider their combined effect as well. In FSW, a semi-quantitative function, the

heat input index (HI), can be expressed [34]:

$$HI = \frac{\omega^2}{v \times 10^3}$$ (1)

where ω is in rpm and v is in mm/min. Fig. 5 (b) shows the relation between heat input and length of kissing bond. As is well known, the heat input during FSW increases with the increasing rotation rate and decreasing the feed rate. Hence, higher heat input conditions which means during the FSW procedure, there are sufficient tool rotation and time to disperse the oxide clusters. It has the same trends shown in Fig. 5 (b) that the L is close to an inversely proportional relationship with HI.
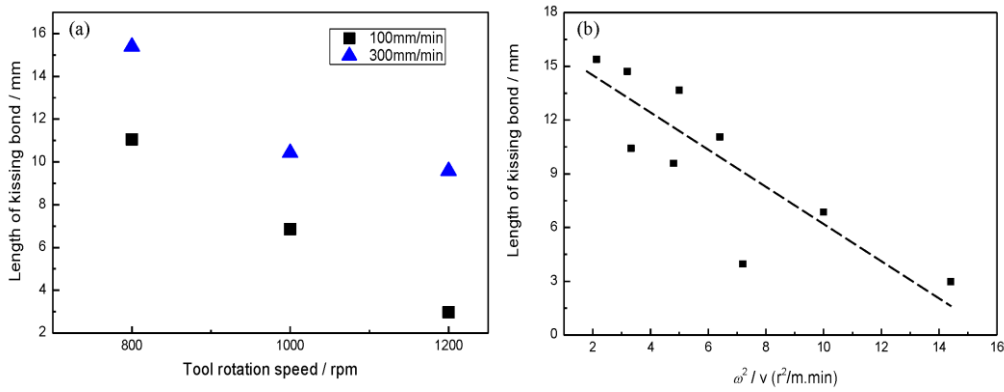

Fig. 5 The effect of welding parameters on the length of kissing bond: (a)- Length of kissing bond (L) vs tool rotation speed ω, (b)-Length of kissing bond (L) vs HI ω^2/v.

3.3 Tensile and fatigue properties of the welds

Fig. 6 shows the ultimate tensile stress (UTS), yield stress (YS) and elongation (EL) of the AA5083 FSW joints, corresponding to different kissing bond lengths. In general, with the increase in kissing bond length, UTS and EL increased first and then decreased. However, YS appeared to show no trend with the kissing bond length. Correlating Fig. 6 with Fig. 5 (b), in other words, it appears that there is no obvious correlation between the YS and the HI.

The Hall-Petch relationship between the grain size (d) and the YS in a polycrystalline material is expressed as:

$$\sigma_{YS} = \sigma_0 + k_y d^{-1/2}$$ (2)

where, σ_0 is the frictional stress contribution, d is the grain size, and k_y is the Hall-Petch slope. It was revealed in Fig.6 (b) that the YS appeared to increase with the increase in the

tool rotation speed. If strength was solely based on grain size strengthening, the grain size in the SZ of the welds should rather decrease with the increase in rotation speed to justify the hardness increase. However, as is shown in Fig. 7, under the same feed rate, the grain size actually increases with the increase in tool rotation speed, possibly due to the higher temperatures in these welds. As such, the increase in YS with the increase in grain size suggests that the contributions of other strengthening mechanisms increase with the increase of rotation speed, especially Orowan strengthening and dislocation strengthening, which were previously reported to contribute to the strength of AA5xxx FSW joints [35, 36]. However, it can be noticed that apart from the 1200rpm samples, the YS of the other samples were lower than that of the base metal (163MPa on average), even though the grain size of the SZ was much finer. Hence, it could be considered that, the welds were homogeneous at the tool rotation speed of 1200rpm, while at 800rpm and 1000rpm, the kissing bond could be considered as a "defect" which had a negative effect on the YS.
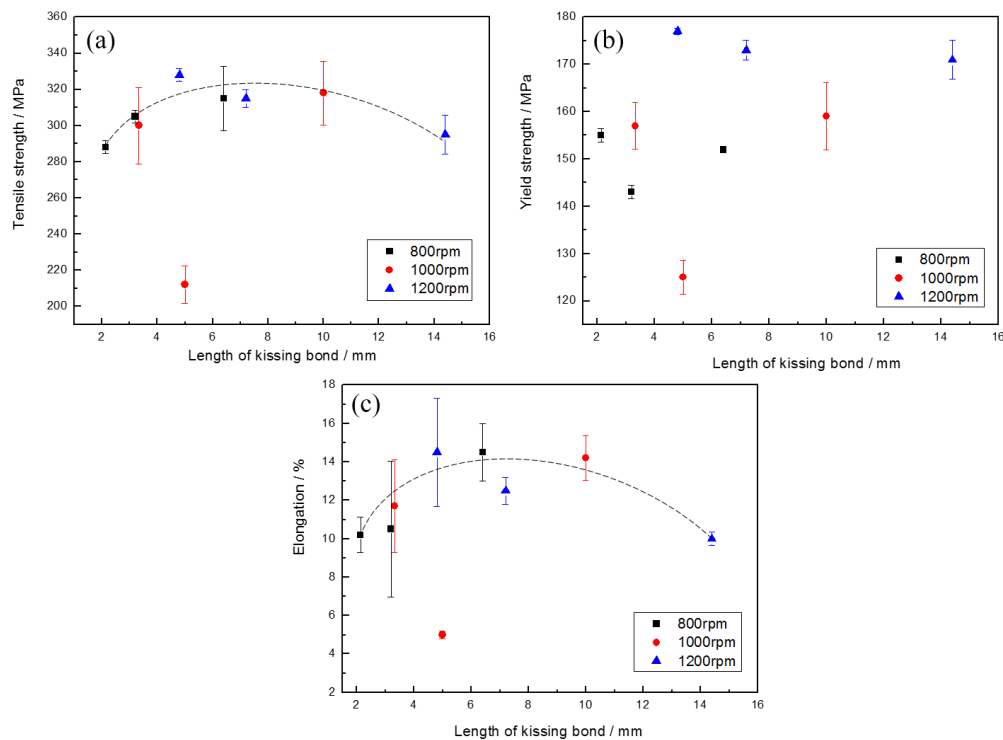

Fig. 6 Tensile properties of AA 5083 FSW joint with different kissing bond lengths.
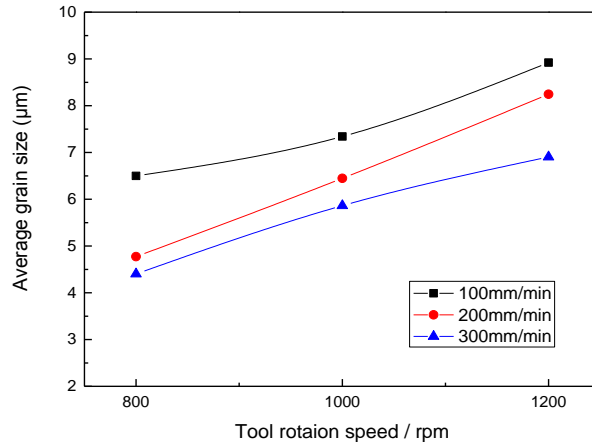(a) Ultimate Tensile Stress, (b) Yield Stress, and (c) Elongation.

10

Fig. 7 Average grain sizes in the SZ of AA5083 FSW joints at different tool rotation speeds.

Fig. 8 shows the fatigue life of different welds as a function of the kissing bond length. The maximum stress used during fatigue testing was kept constant as 130 MPa, which was 70% of the YS for AA5083-H112 base metal, to assess the fatigue fracture behaviour of the welds with different kissing bond lengths. As shown, the fatigue life of the AA5083 FSW joints decreased with the increase in the kissing bond length. The results revealed that the kissing bond length has a negative effect also on the fatigue strength for the welds.
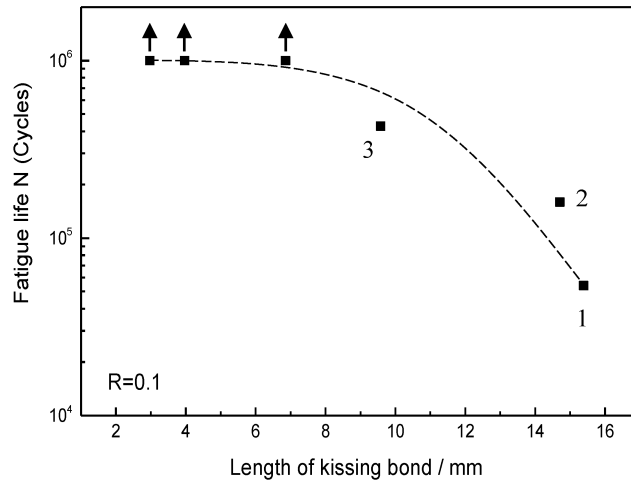

Fig. 8 Fatigue test results for AA5083-H112 FSW joint with different kissing bond lengths.

4. Discussion

4.1 Tensile fracture types

Three types of tensile fracture were observed in the transverse tensile specimens of the AA5083-H112 FSW joints. Fracture type 1, where the fracture location was in the SZ towards AS, was found in the 1200rpm-300mm/min joint (see Fig. 9 (a)). The fracture path was virtually linear throughout the sheet, inclined at ~45°to the tensile loading direction almost as

a pure shear fracture. A C-shaped kissing bond was observed in the SZ towards the RS. This suggests that the crack initiation at the SZ/TMAZ region towards the AS was easier than in the kissing bond region towards RS, which resulted in the fracture being located towards the AS during tensile testing. Fig. 10 (a) shows the fracture surface corresponding to Fig. 9 (a), with the fracture surface consisting of fine equiaxed dimples with various sizes, indicating a ductile failure mode. This condition displayed the highest UTS, YS, and EL (328 MPa, 178 MPa, and 14.5%, respectively) among all the conditions investigated in this research. Compared with the tensile results obtained for the parent material AA5083-H112, (335 MPa, 163 MPa, and 20%), the UTS and EL were slightly lower than the parent metal. However, the YS was virtually similar (~15 MPa higher) to the BM in average, due to the fine recrystallised grains in the SZ.

Fracture type 2 was observed in the 1000 rpm-200 mm/min joint, whereby the fracture was also located in the SZ, initiating from the RS, Fig. 9 (b). The fracture path was characterised by a zigzag path on the top of the weld, extending to a lazy S shape. It was found that the fracture path in type 2 occurred along the kissing bond. However, in this case, the UTS, YS, and EL were the lowest among the welds investigated in this study, with 212 MPa, 125 MPa, and 5% on average, respectively. It is obvious that the presence of a profound kissing bond makes the joints prone to easy crack during tensile testing, because the dislocations could pile-up at the large oxide clusters, which resulted in stress concentration, cracks along the kissing bond and lower tensile stresses.

Fracture type 3 was a hybrid type between the previous two, and could be observed in most cases. The fracture path in this type initiated with a shear fracture, extending along the lazy-S section of the kissing bond, as shown in Fig. 9 (c). The images of fracture surface for fracture type 3 were shown as Fig. 10 (b), (c), and (d). Fig. 10 (b) shows the detailed morphology for fracture type 3 corresponding with shear fracture portion of the fracture path in Fig. 9 (c). It was found that the surface of shear fracture was similar to type 1 in its morphology, showing dimples along the fine grain structure. The difference was that the fine and round dimples in type 1 was deeper than in type 3 (see Fig. 10 (a) and (b)), which was indicated to have lower

tensile properties than samples fractured in type 1. In terms of the surface of the fracture along the kissing bond in Fig. 10 (c), no large dimples could be observed, although few regions showing trench-like fracture regions were observed. Under higher magnification, (Fig. 10 (d)), shows that the trenches contained fine round particles, containing 8.7 at% O, 4.81 at% Mg and 86.49 at% Al, which suggests them to be the oxides particles associated with the kissing bond structure. It is clear that the kissing bond had contributed to the fracture path in type 2 and 3, and to their reduced tensile properties.
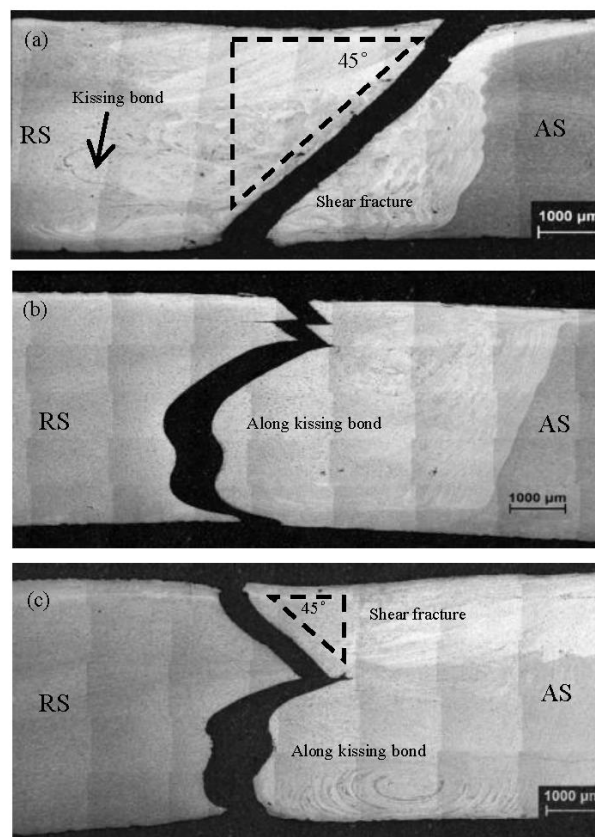

Fig. 9 Macrostructure profiles of the fracture of AA5083-H112 FSW joints.
(a)- ω=1200rpm, v=300mm/min, (b)- ω=1000rpm, v=200mm/min, (c)- ω=1000rpm, v=100mm/min.
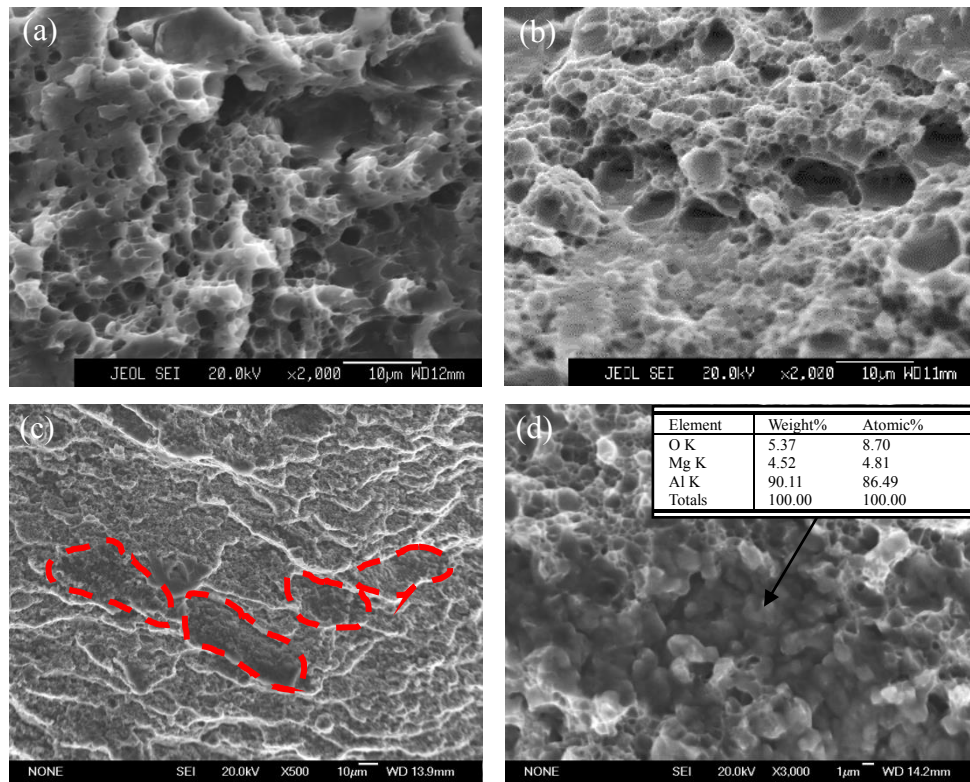
Fig. 10 SEM micrographs for the fracture surfaces of AA5083-H112 FSW joints for (a) type 1, (b) type 3-shear fracture, (c) type 3-along the kissing bond, (d) high magnification of the dotted regions in (c).

4.2 Fatigue behaviour

Fig. 11 (a), (b) and (c) show the fracture surface for the specimens corresponding to point 1, 2 and 3 in Fig. 8. Three distinct regions could be distinguished; crack initiation, crack propagation, and final fracture, which had various sizes for different weld conditions. Generally, the size of the crack initiation and crack propagation regions decreased in the joints showing longer fatigue life. It was noticed that multiple initiations were observed in Fig. 11 (a), (b), which were corresponding to the joints showing shorter fatigue life. These initiations were reported to originate from the kissing bond[18]. Moreover, periodic striations in the crack propagation zone were clearly visible in specimen 1 and 2 (marked in Fig. 12 (a) and (b)). The striations were shown from the multiple crack initiations to the boundary between crack propagation zone and final fracture. It was noticed that the striations of specimen 2 were decreased in width and less clear than specimen 1, however, the striations were not visible in specimen 3. Zettler *et al.* [37] found similar non-chaotic striations or bands associated with the tool advance per revolution along the cross-section along the weld direction in a AA6063-T6 FSW joint. Differently, in this study, the periodic bands shown in Fig. 11 (a) and (b) were

generated due to the fatigue crack propagation. Fig. 11 (d) shows the SEM image observed in the vicinity of a striation in the fatigue fracture. Apart from the macroscopical striation marked in Fig. 11 (d), the micro-scale fatigue striations (a characteristic feature of the fatigue crack propagation) were also visible. Besides, the crack growth direction could be identified as the vertical direction of the fatigue striations[18].
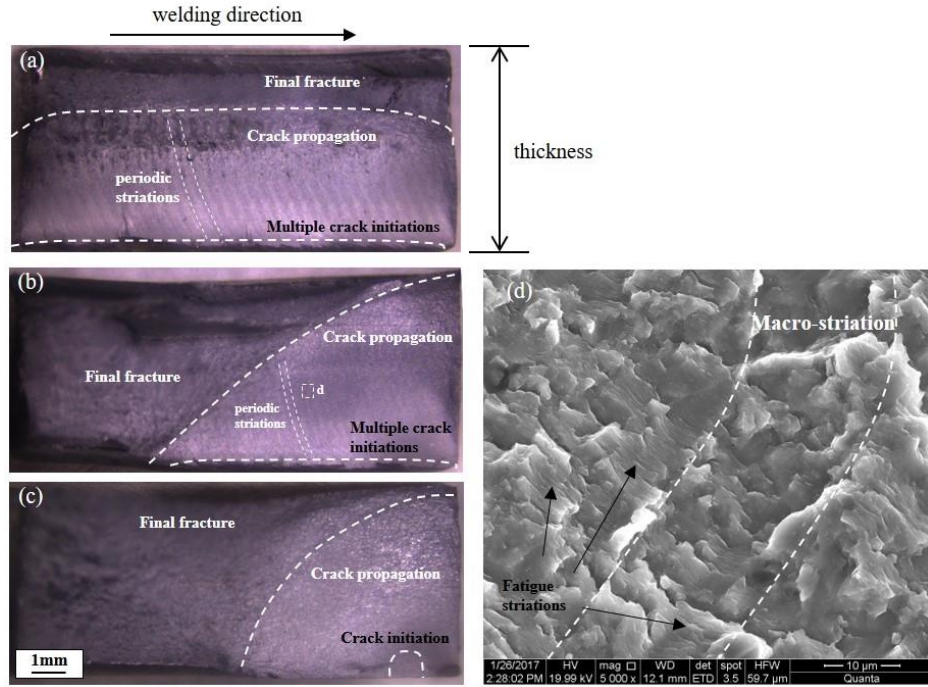

Fig. 11 Macrograph of fractured surface of fatigue specimens corresponding to point 1-(a), 2-(b) and 3-(c) in Fig. 8, and (d)-SEM of crack propagation zone in image (b).

Fig. 12 illustrates the fatigue fracture path collected from both sides of the fatigue specimens corresponding to point 1, 2 and 3 in Fig. 8. It was clearly shown that the fatigue fracture path had a great difference for the welds prepared at various welding parameters. Fig. 12 (a) shows the specimen corresponding to point 1 in Fig. 8. The welding parameters were 800 rpm tool rotation speed and 300 mm/min feed rate. The fatigue fracture path is symmetrical in both sides of the specimen, basically a straight line on the bottom of the specimen, while on the upper part, the fracture path shows a zigzag line which indicates that the final fracture was along the kissing bond. Fig. 12 (b) shows the fatigue fracture path of the specimen, which was obtained at 800 rpm tool rotation speed and 200 mm/min welding speed. As is clearly shown, the fracture path is asymmetrical. The crack initiation part is shown as a straight line from the top to the bottom, normal to the fatigue load direction. While the final fracture path is a zigzag

line, which is similar to the tensile fracture path. Fig. 12 (c) shows the fatigue fracture path of the specimen obtained at 1200 rpm tool rotation speed and 300 mm/min feed rate. The fracture path is also asymmetrical, with the only difference from Fig. 12 (b) being that the final fracture path is a straight-line inclined 45° to the fatigue loading direction (also similar to the tensile fracture path). Therefore, these results revealed that the kissing bond had a significant contribution to the final fracture in the fatigue behaviour. It is clear that with the increase of the kissing bond length in the welds, the area of crack initiation zone increased, affecting the fatigue life of the welds.
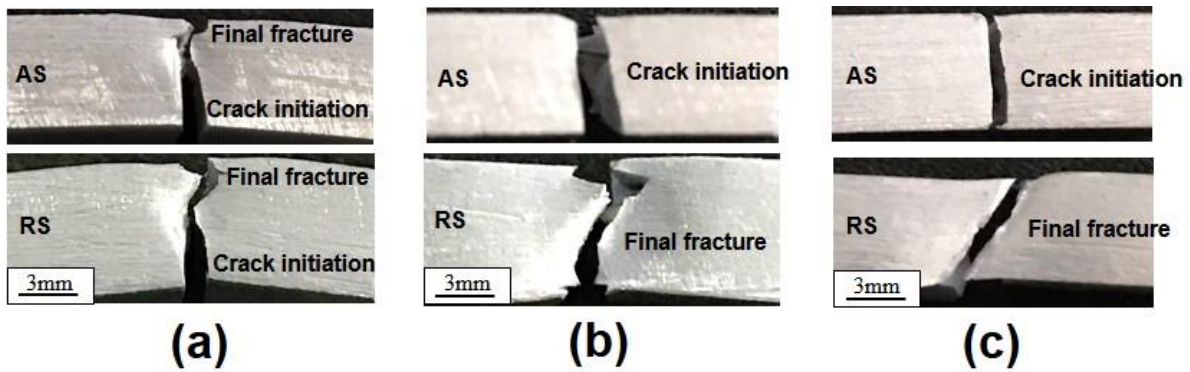

Fig. 12 Fracture path for fatigue specimens corresponding to point 1-(a), 2-(b) and 3-(c) in Fig. 8.

4.3 Correlating the fracture types with the tensile and fatigue properties

The relationship between fracture type and UTS of FSW AA5083 is shown in Fig. 13. The tensile test results revealed that the welds fractured following type 1 had the highest UTS, whereas type 2 was associated with the lowest UTS, and type 3 had average UTS between type 1 and type 2. Generally, the welds fractured in type 3 had acceptable UTS when the HI was in the moderate level (between 5 and 10 r^2/m·min). However, when the HI was above or below that range, the UTS of the welds were relatively lower and the fracture type changed to a combination of type 1 and type 2. Type 2 fracture actually resulted in the lowest UTS. In one occasion, two conditions displaying the same HI (~5 r^2/m·min) were found to yield extremely contrasting UTS, suggesting that the HI is not a reliable parameter to correlate the fracture type with the tensile properties, although it correlates reasonably with the kissing bond length (Fig. 5)
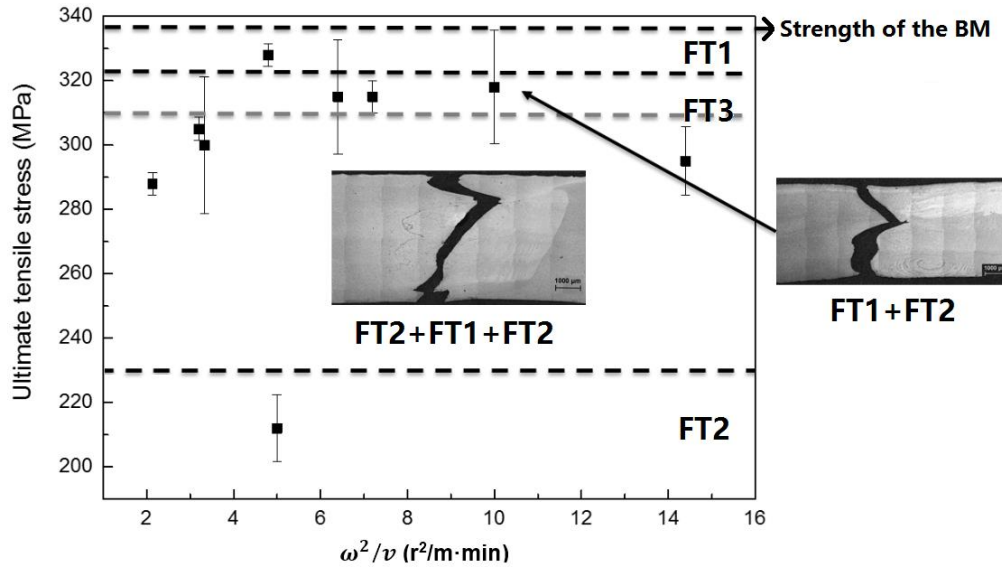
Fig. 13 The relationship between fracture type (FT) and UTS of FSW AA5083.

Similar to the tensile fracture, a shear fracture path due to fatigue loading had a longer fatigue life, whereas the path along the kissing bond was associated with a shorter fatigue life. The increase in the kissing bond length reduced the area of the final fracture region and enlarged the area of crack initiation, which resulted in a shorter fatigue life.

5. Conclusions

In this study, 6 mm AA5083-H112 friction stir butt welds were prepared using different welding parameters combinations. The kissing bond length in the welds was quantitatively measured, studying its influence on the tensile and fatigue properties of the welds and the process parameters interactions. Besides, the tensile and fatigue properties and fracture types and their relationship with the process parameters were studied. The following conclusions were drawn:

- The length of the kissing bond was found to have a reasonably linear relation with the heat input (HI), which depends on the tool rotation speed and feed rate.
- With the increase in the length of the kissing bond, the tensile UTS and EL increased first and then decreased, while the YS had no obvious trend with the kissing bond length. Besides, the fatigue life of the welds was longer with the shorter kissing bond.
- The tensile UTS and fatigue life of the welds were strongly correlated with the fracture types. The shear fracture resulted in higher tensile UTS and longer fatigue life, while poor

strength and fatigue properties were associated with the welds showing a fracture path along the kissing bond.

References

[1] Y. Birol, S. Kasman, Materials Science and Technology, 29 (2013) 1354-1362.

[2] S. Kimura, T. Wakisaka, I. Katou, T. Goto, H. Machida, Journal of Japan Institute of Light Metals, 57 (2007) 554-558.

[3] R. Kumar, K. Singh, S. Pandey, Transactions of Nonferrous Metals Society of China, 22 (2012) 288-298.

[4] P.A. Colegrove, H.R. Shercliff, R. Zettler, Science and Technology of Welding and Joining, 12 (2007) 284-297.

[5] C.-H. Chien, W.-B. Lin, T. Chen, Journal of the Chinese Institute of Engineers, 34 (2011) 99-105.

[6] D.-H. Choi, B.-W. Ahn, D.J. Quesnel, S.-B. Jung, Intermetallics, 35 (2013) 120-127.

[7] K. Dudzik, M. Czechowski, Solid State Phenomena, 220-221 (2015) 583-588.

[8] T. Hirata, T. Oguri, H. Hagino, T. Tanaka, S.W. Chung, Y. Takigawa, K. Higashi, Materials Science and Engineering: A, 456 (2007) 344-349.

[9] J.K. Paik, International Journal of Naval Architecture and Ocean Engineering, 1 (2009).

[10] M. Peel, A. Steuwer, M. Preuss, P.J. Withers, Acta Materialia, 51 (2003) 4791-4801.

[11] D. Rao, K. Huber, J. Heerens, J.F. dos Santos, N. Huber, Materials Science and Engineering: A, 565 (2013) 44-50.

[12] C. Zhou, X. Yang, G. Luan, Scripta Materialia, 53 (2005) 1187-1191.

[13] H. Lombard, D.G. Hattingh, A. Steuwer, M.N. James, Engineering Fracture Mechanics, 75 (2008) 341-354.

[14] M. Grujicic, G. Arakere, H.V. Yalavarthy, T. He, C.F. Yen, B.A. Cheeseman, Journal of Materials Engineering and Performance, 19 (2009) 672-684.

[15] P.L. Threadgill, A.J. Leonard, H.R. Shercliff, P.J. Withers, International Materials Reviews, 54 (2013) 49-93.

[16] S.R. Ren, Z.Y. Ma, L.Q. Chen, Materials Science and Engineering: A, 479 (2008) 293-299.

[17] H. Okamura, K. Aota, M. Sakamoto, M. Ezumi, K. Ikeuchi, Welding International, 16 (2002) 266-275.

[18] M. Kadlec, R. Růžek, L. Nováková, International Journal of Fatigue, 74 (2015) 7-19.

[19] T. Le Jolu, T.F. Morgeneyer, A. Denquin, M. Sennour, A. Laurent, J. Besson, A.-F. Gourgues-Lorenzon, Metallurgical and Materials Transactions A, 45 (2014) 5531-5544.

[20] N.Z. Khan, A.N. Siddiquee, Z.A. Khan, S.K. Shihab, Journal of Alloys and Compounds, 648 (2015) 360-367.

[21] Y.S. Sato, H. Takauchi, S.H.C. Park, H. Kokawa, Materials Science and Engineering: A, 405 (2005) 333-338.

[22] G. Staniek, M. Schmucker, T. Vugrin, Welding and cutting, 4 (2005) 271-276.

[23] H.L. Hao, D.R. Ni, H. Huang, D. Wang, B.L. Xiao, Z.R. Nie, Z.Y. Ma, Materials Science and Engineering: A, 559 (2013) 889-896.

[24] T. Morita, M. Yamanaka, Materials Science and Engineering: A, 595 (2014) 196-204.

[25] Y. Tao, Z. Zhang, D.R. Ni, D. Wang, B.L. Xiao, Z.Y. Ma, Materials Science and Engineering: A, 612 (2014) 236-245.

[26] J. Yang, D. Wang, B.L. Xiao, D.R. Ni, Z.Y. Ma, Metallurgical and Materials Transactions A, 44 (2012) 517-530.

[27] C. Zhou, X. Yang, G. Luan, Journal of Materials Science, 41 (2006) 2771-2777.

[28] T. Le Jolu, T.F. Morgeneyer, A. Denquin, A.F. Gourgues-Lorenzon, International Journal of Fatigue, 70 (2015) 463-472.

[29] Z. Zhang, B.L. Xiao, Z.Y. Ma, Metallurgical and Materials Transactions A, 44 (2013) 4081-4097.

[30] British Standerd Institution, 389 Chiswick High Road, London, UK, 2001.

[31] ASTM International, West Conshohocken, PA, USA, 2007.

[32] S. Di, X. Yang, G. Luan, B. Jian, Materials Science and Engineering: A, 435-436 (2006) 389-395.

[33] H.-B. Chen, K. Yan, T. Lin, S.-B. Chen, C.-Y. Jiang, Y. Zhao, Materials Science and Engineering: A, 433 (2006) 64-69.

[34] V. Dixit, R.S. Mishra, R.J. Lederich, R. Talwar, Science and Technology of Welding and Joining, 12 (2013) 334-340.

[35] M.M. Attallah, M. Strangwood, C.L. Davis, Scripta Materialia, 63 (2010) 371-374.

[36] Y.S. Sato, S.H.C. Park, H. Kokawa, Metallurgical and Materials Transactions A, 32 (2001) 3033-3042.

[37] R. Zettler, 3 - Material deformation and joint formation in friction stir welding, Friction Stir Welding, Woodhead Publishing, 2010, pp. 42-72.